

RESEARCH ARTICLE

Waste biomass gasification char derived activated carbon for pharmaceutical carbamazepine removal from water

Ming-Ho To¹ Pejman Hadi¹ Chi-Wai Hui¹ Carol Sze Ki Lin^{1,2} Tareq AI-Ansari³
Junaid Saleem³ Prakash Parthasarathy³ Gordon McKay^{3*}

Abstract: Carbamazepine (CBM), a widely occurring pharmaceutical, has been removed from water by upgrading a waste biomass char from a 300 MW biomass gasification power station plant operating in Indonesia. The fuel source is the waste residue palm kernel shell (PKS) after the palm oil extraction process constituting over one million tonnes per year. The resulting waste power station biomass char (CPKS) from the power station gasification process has been converted into a high quality activated carbon by carbon dioxide activation as a sequestration opportunity, at different temperatures ranging from 700 to 900°C for 1 or 1.5 hours. The highest BET surface area was 711.5 m²/g and this activated carbon was able to adsorb 1.14 mmol/g or 268.7 mg CBM/g. Equilibrium and kinetic studies have been undertaken.

Keywords: biomass power station residue, activated carbon, PPCP carbamazepine removal, capacity and kinetic studies

1 Introduction

Adsorption of pollutants via activated carbon is a good candidate for wastewater treatment without producing undesirable side products. It is widely used in pollution treatment for heavy metals^[1,2], dyes^[3], and pharmaceuticals^[4]. Activated carbons are produced using bone char^[5], peat^[6], fly ash^[7], bamboo^[8], pine cone^[9], and palm oil shell^[10], which possess high adsorption capacities. The demand for activated carbons is increasing; so new, cheap and abundant precursor materials are needed. Besides, agricultural by-products such as silk cotton hull, coconut tree sawdust, bagasse pith, macadamia nut, pine wood were also used to produce activated carbon for the adsorption of heavy metals, dyes, and pharmaceutical wastes^[3,11-15]. Other waste materials have been used for heavy metals and dyes^[16] and more expensive adsorbents

such as chitosan have been applied for the pharmaceutical acetaminophen removal^[17].

Activation can be chemical, when both carbonization and activation are combined, using alkalis, acids or zinc chloride developing higher porosity and functionality, or physical methods^[12]. However, using such activating agents produces some environmental pollution. Therefore, often the physical activation method is preferable which involves the carbonization and activation steps. In the carbonization stage, the temperature is in the range between 400 and 850°C in an inert gas (*e.g.* nitrogen) to enrich the carbon content and generate the initial porosity. During activation, the temperature is further increased to between 600 and 900°C where gasification occurs by reaction between the carbonaceous material and the oxidizing gas (*e.g.* carbon dioxide and/or steam), developing well-developed internal pore structure.

Palm kernel shell (PKS) is an agricultural waste product from the palm oil industry. After oil extraction, the residual palm kernel shell (PKS) biomass is processed by gasification in the palm oil mill or more recently for power generation^[18]. In the past decade, the PKS waste by-product has been proposed as a precursor source for activated carbon. Lua and Guo^[19] studied the activation of PKS by CO₂ and they performed further experiments to identify the optimum pyrolysis conditions of 600°C for 2 hours in nitrogen.

In the present work, the waste PKS char has been taken and separated into two fractions by sieving. The proper-

Received: Sept. 1, 2019; Accepted: Sept. 16, 2019; Published: Sept. 18, 2019

*Correspondence to: Gordon McKay, Division of Sustainability, College of Science and Engineering, Hamad Bin Khalifa University, Qatar Foundation, Doha, Qatar; Email: gmckay@hbku.edu.qa

¹ Chemical and Biomolecular Engineering Department, Hong Kong University of Science and Technology, Clear Water Bay Road, Hong Kong

² School of Energy and Environment, City University of Hong Kong, Tat Chee Avenue, Kowloon, Hong Kong

³ Division of Sustainability, College of Science and Engineering, Hamad Bin Khalifa University, Qatar Foundation, Doha, Qatar

Citation: To MH, Hadi P, Hui CW, *et al.* Waste biomass gasification char derived activated carbon for pharmaceutical carbamazepine removal from water. *Resour Environ Inf Eng*, 2019, 1(1): 36-44.

Copyright: © 2019 Gordon McKay, *et al.* This is an open access article distributed under the terms of the [Creative Commons Attribution License](https://creativecommons.org/licenses/by/4.0/), which permits unrestricted use, distribution, and reproduction in any medium, provided the original author and source are credited.

ties and applications of the combusted part of the gasification residue has been reported^[18]. The carbonaceous char fraction (CPKS) was sieved into different size ranges (*i.e.* ≤ 0.15 mm, 0.5-0.71 mm and 1-1.4 mm) and the activation of those samples will be undertaken by carbon dioxide at different temperatures. The resultant activated materials were then characterized by BET surface area analysis and the adsorption characteristics were determined by the adsorption of the pharmaceutical compound carbamazepine in aqueous solution. Pharmaceutically active compounds and personal care pharmaceutical products, PPCPs, typified by carbamazepine, have been detected in treated sewage effluent and our drinking water treatment plants which is a major cause of concern. Treatment by carbon adsorption^[20] using a waste material offers an attractive solution.

2 Material and Methods

2.1 Chemicals

The starting material used in this work is the biomass char retained sieved fraction from the Indonesian Biomass Power Station at Tanjung Batu, - the charred biomass of palm kernel shell (CPKS) kindly supplied by the power station design and installation consortium company Peako Engineering Co., Limited, Hong Kong and Biomass Energy Co., Ltd. Jiangxi Peako, Pingxiang City, Jianxi Province, China.

Sodium hydroxide (NaOH), hydrochloric acid (HCl, 37%) and ammonium acetate (NH₄Ac) were purchased from Sigma-Aldrich as well as pharmaceutical grade carbamazepine (CBM, C₁₅H₁₂N₂O), which is an antiepileptic drug, with a molecular weight of 236.3 g/mol and a pK_a = 13.9. The solvents (ethanol (C₂H₆O) and acetonitrile (CH₃CN)) are HPLC grade and obtained from VWR.

2.2 Instrumentation

The HPLC instrument (HPLC, 2695 separation module, waters®) equipped with a model 2996 Photodiode Array Detector was employed. Separation and quantization were obtained from Accucore XL C18 Thermo® using a 150 x 4.6 mm column with particle size of 4 μ m. Data acquisition was performed on a Empower™ Software.

2.3 Sample Preparation

The starting material used in this work is the charred palm kernel shell (CPKS) and its surface area was 255.8 m²/g as determined by a BET analyzer (SA3100, Beckman Coulter). The activation process is similar to Lua's procedure with minor modification^[19]. In brief, the start-

ing material was first crushed and sieved to different size (≤ 0.15 mm, 0.5-0.71 mm and 1-1.4 mm) according to the particle size for PAC, GAC and EAC mentioned in the ASTM guideline. The activation process was carried out in a quartz tube in a vertical tube furnace (Eurotherm 2408). Approximately 5 g of the CPKS raw material was weighed in a quartz boat and transferred into the quartz tube which was then inserted in to the tube furnace for activation. The CPKS was heated with a ramp rate of 5°C/min to the activation temperature (700 to 900°C) and held for 1 or 1.5 hours in a N₂ and CO₂ gas sweep at a flow rate of 50 cm³/min.

2.4 Sample structure analysis

The porosity and the surface area of the activated CPKS were determined by nitrogen adsorption at -196°C using a BET surface area analyzer (SA3100, Beckman Coulter). A sample of 0.1 g was first outgassed at 200°C for 3 hours. The Brunauer-Emmett-Teller (BET) and Barrett-Joyner-Halenda (BJH) models were used to study the specific surface area, micropore volume, and the external surface area and porosity. The point of zero charge, pH_{pzc} of the adsorbent was determined using 50 ml of 0.01 M NaCl solution dispensed to Erlenmeyer flasks. Then, the initial pH was adjusted to between 2 to 13 by HCl and NaOH solution. 0.2 g of the adsorbent was added to each flask and shaken at 250 rpm for 48 hours at 25°C and the final pH was recorded. The pH_{pzc} was then determined at the intersection of the curve pH_{final} versus pH_{initial} overlapped the straight line corresponding to pH_{initial} = pH_{final}.

2.5 Kinetic adsorption studies

The time to reach equilibrium was determined by kinetic adsorption studies. Several 200 ml samples of CBM solutions at 100, 150, 200 and 250 ppm were prepared by diluting a 700 ppm CBM stock solution. The initial pH values of the solutions were adjusted to 7 by HCl and NaOH, then 0.2 g activated CPKS was added to each solution and agitated at 250 rpm in a rotary shaker at 25°C. The adsorption kinetics were studied by measuring the decrease in CBM concentration at time intervals from initial until the equilibrium adsorption was reached.

2.6 Isotherm adsorption study

Equilibrium isotherms of the CPKS adsorbents were determined using batch adsorption experiments. A stock CBM solution was prepared by ultrapure water with 10% ethanol (to increase the solubility of the CBM). 50 ml of the CBM at different concentrations were prepared by diluting the 700 ppm stock solutions. The pH of the

solutions were adjusted to 7, 50 mg adsorbent was then added to 50 ml CBM working solution and agitated at 250 rpm in a rotary shaker at 25°C for 24 hours. The change in CBM concentration before and after the adsorption experiment was determined by HPLC.

The adsorption capacity at the equilibrium q_e (mg/g) was calculated by Equation (1)

$$q_e = \frac{(C_o - C_e) V}{W} \quad (1)$$

where C_o and C_e (mg/L) represent the initial and equilibrium CBM concentrations, respectively, V and W are the volume of the solution (L), and the mass of dry adsorbent used (g).

2.7 CBM concentration analysis

The change in CBM concentration in the batch and kinetic adsorption experiments was determined by high performance liquid chromatography (HPLC). In which, 2 ml of the aspirated sample from the experiment was first filtered through a 0.22 μm polytetrafluorethylene (PTFE) syringe filter (Millipore, Milford, MA, USA). The mobile phase for the HPLC was prepared by mixing ammonium acetate and acetonitrile in a ratio of 72:28 v/v. The analysis was performed at 25°C, using 5 μl sample and a flow rate of 1.5 ml/min.

2.8 Data analysis

The adsorption kinetics were analyzed by testing five models including pseudo-first-order, pseudo-second-order, Elovich, Modified second, and Ritchie second order model. The adsorption isotherms were analyzed by Langmuir, Freundlich, Sips, Redlich-Peterson and Temkin isotherm models. The variables of each model were determined by the solver function of Microsoft Office Excel program. The model parameters for each isotherm were calculated by the respective equations. The difference between the experimental data and the data calculated from the models was used to calculate the sum of the error squares (SSE) (Equation (2)) to obtain the best fit isotherm constants.

$$SSE = \sum (q_{exp} - q_{cal})^2 \quad (2)$$

3 Results and discussion

3.1 Mass yields of the activated products

The yields of the activated materials are shown in Table 1. The percentage yields representing the decrease in weight after the carbon dioxide activation process are also shown. The yield decreased from 85% to 55% as the

activation temperature increased from 700 to 900°C and held for 1 hour. When the holding time increased from 1 hour to 1.5 hour, the yield was further decreased by 18% to 37%. The yield of the activated product also decreased according to the precursor particle size. The finer the precursor's particle size, the lower the percentage yield. The reduction in weight during the activation process was ascribed to the carbon burn off through the oxidation of carbonaceous material by CO_2 therefore resulting in the release of volatile matter and forming a porous structure in the carbonaceous material. More significant carbon- CO_2 reactions occur when the activation temperature increased from 700 to 900°C and extending the time of activation from 1 hour to 1.5 hour caused significant reduction in the percentage yield.

The yield of the activated carbon decreased with increasing the temperature and activation duration. An increase in particle size also increased the final yield.

3.2 Textural properties of PKS

The characteristic of the activated PKS was determined by BET surface area analysis as shown in Table 1. By keeping the activation time constant at 1 hour, the SBET surface area increased from 700°C at 379°C to 496.8 m^2/g at 800°C. A further increase in the SBET surface area to (617.4 m^2/g) almost double was observed, when the activation temperature was increased to 900°C. In addition, while keeping the activation temperature at 900°C and extended the holding time from 1 hour to 1.5 hours further improved the BET surface area from 617.4 to 711.5 m^2/g suggesting that the activation temperature is more important in the porous structure formation. Besides, the particle size of the precursor for carbon dioxide activation also had an inverse effect on the resultant BET surface area of the activated material. When the activation condition was kept at 900°C for 1.5 hours, the final BET surface area reduced depending on the particle size. It reduced from 711.5 m^2/g (size ≤ 0.15 mm) to 352.8 m^2/g (size 0.5-0.71 mm) and further reduced to 274.4 m^2/g (size 1-1.4 mm), the smaller the particles size results in a larger surface area therefore produced more adsorption sites^[21].

Other than the surface area, the total porosity also increased with the activation temperature. In Figure 1, when the activation temperature increased from 700 to 800°C, a small increase in the porosity from 22% to 24% was observed. In contrast, a more significant change was observed when the activation temperature rose to 900°C which caused an increase of 11% in porosity, reaching 35%. Further improvement in the porosity was seen by increasing the duration of activation from 1 to 1.5 hours and so obtaining the highest porosity of 42%. The increase in

Table 1. The textural properties of the activated CPKS. The surface area, SBET, and total porosity, Pv, increased with the activation temperature and duration of activation. There is an obvious drop in surface area and total porosity, when the particle size increased to 1-1.4 mm. MESA: mesopore surface area; dp pore diameter; Mv: mesopore volume; BJH: Brunnauer-Joyner-Halenda method

Sample	SBET m ² g ⁻¹	Total Pv volume cm ³ g ⁻¹	t-plot Mv cm ³ g ⁻¹	Mesopore volume cm ³ g ⁻¹	t-plot MESA m ² g ⁻¹	Adsorption av. Dp/ Desorption av. Dp BJH Å	Mass % product yield
700°C 1h size ≤0.15 mm	379	0.219	0.130	0.089	96.0	0.0538/ 0.0405	85
800°C 1h size ≤0.15 mm	497	0.214	0.154	0.061	99.8	0.0448/ 0.0412	78
900°C 1h size ≤0.15 mm	617	0.351	0.204	0.147	168.4	0.0843/ 0.0887	55
900°C 1.5h size ≤0.15 mm	712	0.419	0.236	0.183	199.6	0.1830/ 0.1086	52
900°C 1.5h size 0.5-0.71 mm	353	0.209	0.102	0.108	128.4	0.0570/ 0.0607	44
900°C 1.5h size 1-1.4 mm	274	0.172	0.051	0.121	49.2	0.0290/ 0.0240	37

porosity was proportional to the degree of the Boudouard reaction which is a temperature dependent reaction ($\Delta H = 172 \text{ kJ/mol}$). The reaction involves carbon dioxide and carbon producing carbon monoxide. ($\text{CO}_{2(g)} + \text{C}_{(s)} \rightleftharpoons 2\text{CO}$).

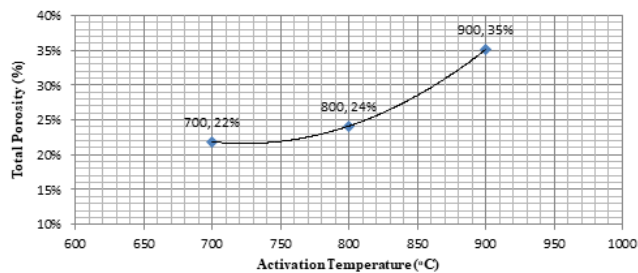


Figure 1. The effect of activation temperature on total porosity formation

When the temperature was $> 700^\circ\text{C}$, the CO formation is more favourable since the free energy change becomes negative. The effect of particle size on porosity was obvious, with decreasing the particle size to the EAC level (size 1-1.4 mm), a significant drop in porosity to 17% was recorded, which was far lower than that of the PAC level (size $\leq 0.15 \text{ mm}$) activated at 700°C for 1 hour. This drop occurred because fewer CO_2 molecules can penetrate into the deeper pores of the larger size particles (size 1-1.4 mm), and therefore lowering the rate of the Boudouard reaction. In addition, a stepwise increase in porosity was

observed when the particle size was 0.5-0.71 mm (GAC level) yielding a 21% porosity value and for the size at $\leq 0.15 \text{ mm}$ (PAC level) reaching the 42% porosity value shown in Figure 2.

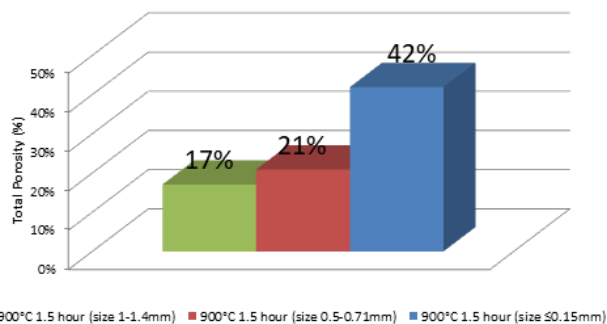


Figure 2. The effect of particle size on the total porosity formation

The pore size distribution of the activated carbons is shown in Figure 3. When the activation temperature was increased, the micropore portion decreased and simultaneously the macropore also increased. The effect of a high pyrolysis temperature in the range, $700\text{-}900^\circ\text{C}$, a softening and sintering of high molecular weight volatiles occurred, resulting in a depolymerisation of the melt and a decrease in the micropore volume of the sample. Hadi *et al.*^[2] demonstrated that a higher activation temperature provided more energy for the reaction between the oxidizing agent (CO_2) and the carbon atom; this led to the

formation of new pores and enlargement of the existing pores. When the reaction was sufficiently fast, micropores could be enlarged to form mesopores. Interestingly, an inverse trend appeared when the activation duration was increased from 1 to 1.5 hours at 900°C indicating that the micropore development was much faster than micropore to mesopore enlargement^[2].

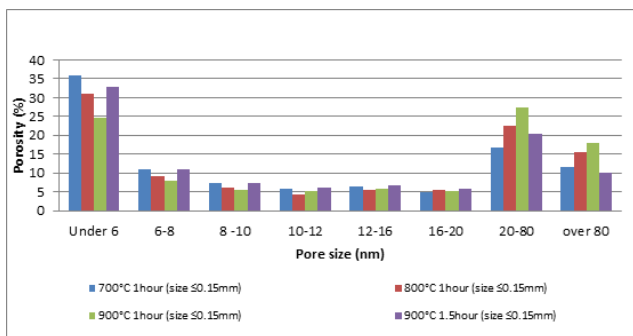


Figure 3. The effect of activation temperature on pore size distribution

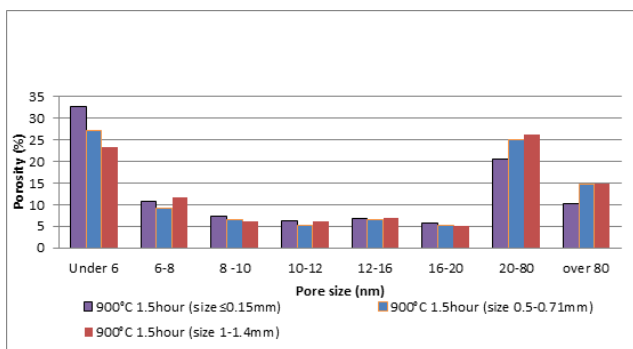


Figure 4. The effect of the precursor particle size on the final pore size distribution

Although the above phenomenon was also applicable in EAC, GAC, and PAC sized materials activated under the same conditions. However, the increased Boudouard reaction promoted by the large surface area, due to small particle size, making it more difficult for the CO₂ molecules to diffuse into the deeper pores of the larger particles for the reaction to have such an overwhelming effect and therefore generating a decrease in the micropore portion of the larger size particle (*i.e.* 0.5-0.71 mm and 1-1.4 mm) as shown in Figure 4.

The nitrogen adsorption-desorption curves of PKS activated at different conditions are shown in Figure 5. All the adsorption-desorption results exhibited a type IV isotherm. Nitrogen adsorption was rapid and the adsorption capacity increased with an increase in pressure as observed in the low pressure region where $p/p_o \leq 0.1$ indicating the contribution of micropores in adsorption.

A hysteresis loop was generated at the high pressure region, which is caused by the capillary condensation of the adsorbate in the mesopores. The hysteresis loop belongs to H4 type isotherm according to the International Union of Pure and Applied Chemistry (IUPAC) classification, indicating a slit-shaped mesoporous material. The adsorption platform is described by the surface area which can be modulated by increasing the activation temperature and duration for the activation process. Therefore, the PKS activated at 900°C for 1.5 hours obtained the highest adsorption platform (of $\sim 260 \text{ cm}^3/\text{g}$). When lowering the activation temperature to 700°C (for 1 hour) the N₂ adsorption surface area was reduced to 140 m²/g. Besides, compared with the EAC and GAC materials, the PAC precursor particle size offered a larger surface area and contributed a significant influence on the adsorption-desorption isotherm.

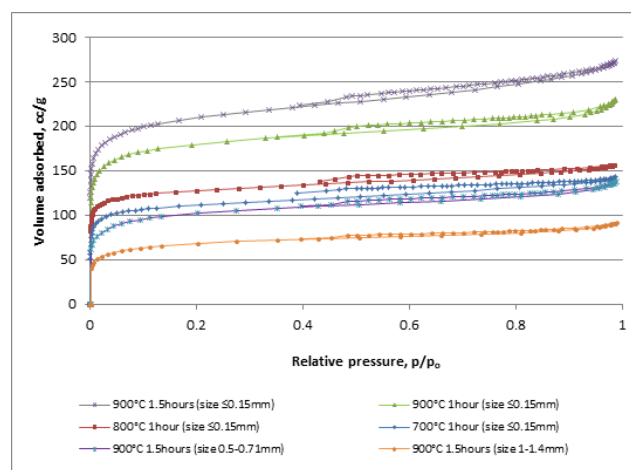


Figure 5. Nitrogen adsorption-desorption isotherm of the activated materials

3.3 Kinetic adsorption study of CBM

Figure 6 shows the kinetic adsorption results for CBM adsorption by the PKS activated carbon. The adsorption capacity increased rapidly for the first 3 minutes and kept increasing with time until a plateau at around 240 minutes reaching the highest equilibrium adsorption capacity of 0.61 mmol/g. To determine the best model to describe the adsorption rate behaviour of CBM on activated PKS, five kinetic models (pseudo first order, pseudo second order, modified second order, Elovich, and Ritchie second order) were used to model with our data.

The pseudo first order kinetic model^[22] can be defined by the Equation (3):

$$q_t = q_e(1 - e^{-k_1 t}) \quad (3)$$

Where q_e is the adsorbate adsorbed (mmol/g) at the

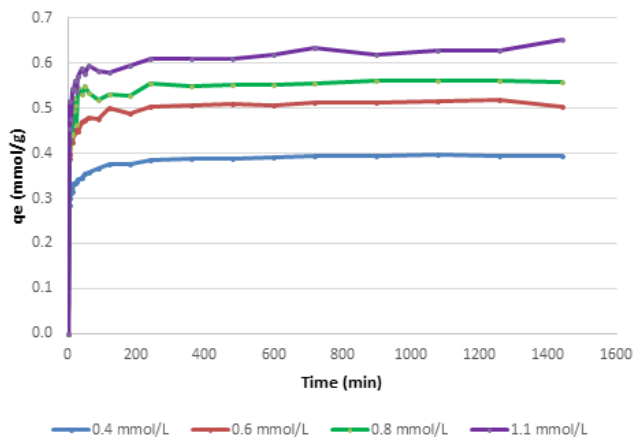


Figure 6. Kinetic adsorption of CBM in 24 hours by adsorbent (size $\leq 0.15\text{mm}$) activated at 900°C for 1.5 hours

equilibrium, q_t is the adsorbate adsorbed (mmol/g) at time t (min), and k_1 is the pseudo-first order rate constant (1/min).

The pseudo-second order kinetic model^[23] can be defined by the Equation (4):

$$q_t = \frac{q_e^2 k_2 t}{1 + q_e k_2 t} \tag{4}$$

Where k_2 is the pseudo-second order rate constant (g/mmol.min).

The Ritchie-second-order^[24] equation can be expressed as in the Equation (5):

$$q_t = q_e \left[1 - \left(\frac{1}{\beta_2 + k_R t} \right) \right] \tag{5}$$

Where k_R is the Ritchie-second-order rate constant (1/min), β_2 represents the surface coverage of the adsorbent.

The Elovich^[25] Equation (6) is given as:

$$q_t = \alpha \ln(a\alpha) + \alpha \ln t \tag{6}$$

Where a and α are the Elovich constants in $\text{mmol min}^{-1}\text{g}^{-1}$ and mmol g^{-1} respectively.

The modified second order equation is given as Equation (7):

$$q_t = q_e \frac{kt + \beta - 1}{kt + \beta} \tag{7}$$

Where k_{2M} is the second order rate constant (min^{-1}) and β is the constant that represents the initial particle loading.

Table 2 shows the calculated parameters for the CBM adsorption on the CPKS (size $\leq 0.15 \text{ mm}$) activated at 900°C for 1.5 h. From the SSE estimated by MS Excel’s solver function, the adsorption of CBM by activated PKS

is most likely represented by the Ritchie-second-order model indicating the rate of CBM adsorption is mainly determined by the fraction of sites which are unoccupied initially and chemisorption of CBM molecule occurred onto the two surface sites of the activated PKS^[5].

Table 2. Kinetic parameters for the adsorption of 1.1 mmol/L CBM ($C_0 = 1.10 \text{ mmol/L}$) onto CPKS activated at 900°C for 1.5 hours

Kinetic Model	Rate Parameter	Equation Constant	$q_{e(\text{calc})}$ (mg/g)	SSE
Pseudo-first order	$k_1 = 1749$ (L/min)	-	0.6	3130
Pseudo-second order	$k_2 = 2804$ (L/min)	-	0.6	3130
Modified second order	$k_{2M} = 13.6$ (L/min)	-	0.6	2130
Ritchie second order	$k_R = 1870$ (L/Min)	$B_R = 78.3$	0.6	0.00067
Elovich	$\alpha = 0.022$ (mg/min/g)	$a = 0.015$ (mg/g)	-	880

3.4 Batch adsorption equilibrium study of CBM

The 24 hours batch adsorption study of CBM by CPKS activated carbon at different conditions are shown in Figure 7. The adsorption capacity at equilibrium increased with the activation temperature and duration reaching the highest value of 0.94 mmol/g by adsorbent activated at 900°C for 1.5 h. The best result was analyzed by five isotherm models (i.e. Langmuir, Freundlich, Sips, Redlich-Peterson, and Temkin isotherm model)^[6] and the parameters were determined by the non-linear regression method in terms of SSE.

The Langmuir model can be defined by Equation (8):

$$q_e = \frac{K_L C_e}{1 + \alpha_L C_e} \tag{8}$$

Where q_e (mmol/g) is the concentration of adsorbate in the adsorbent and C_e (mmol/L) representing the adsorbate concentration remain the solution at equilibrium, α_L and K_L is the Langmuir isotherm constant which is related to the affinity of binding sites.

The Freundlich model can be defined by Equation (9):

$$q_e = \alpha_F C_e^{\frac{1}{n_F}} \tag{9}$$

α_F (mmol/g) (L/mmol) n is the adsorption capacity and $1/n_F$ is the dimensionless intensity of the adsorbent parameter.

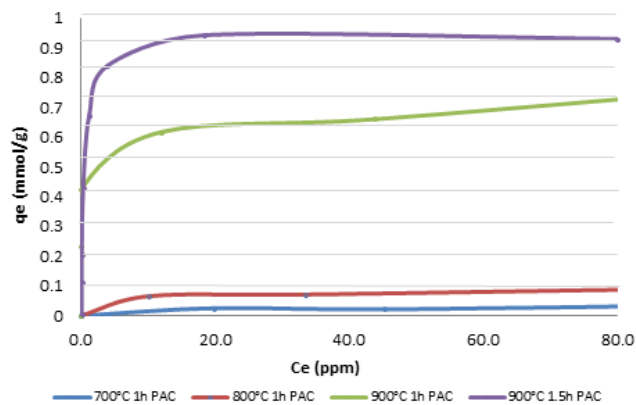


Figure 7. Adsorption isotherms of CBM on the PKS PAC for the three temperatures: 700, 800, 900°C; and for two activation times: 1.0 and 1.5 hours at 900°C

The Sips (Langmuir-Freundlich) model can be defined by Equation (10):

$$q_e = \frac{K_{lf} C_e^{\frac{1}{n_{lf}}}}{1 + \alpha_{lf} C_e^{\frac{1}{n_{lf}}}} \quad (10)$$

Where K_{lf} (L/g) and α_{lf} are the Sips isotherm model constant (L/mmol) and $1/n_{lf}$ is the Sips isotherm exponent.

The Redlich-Peterson model can be defined by Equation (11):

$$q_e = \frac{K_R C_e}{1 + \alpha_R C_e^{\beta_R}} \quad (11)$$

Where K_R (L/g), and α_R (l/ mmol) are the Redlich-Peterson isotherm constants and β_R is the Redlich-Peterson isotherm model exponent.

The Temkin model can be defined by Equation (12):

$$q_e = \frac{RT}{b_T} \ln(A_T C_e) \quad (12)$$

Where R is the universal gas constant (8.314 J/mol°K), T is the absolute temperature (°K), b_T is the Temkin isotherm constant, A_T is the Temkin isotherm equilibrium binding constant, (L/mmol).

The calculated parameters and SSE for CBM adsorption onto activated CPKS are shown in Table 3. The SSE of Redlich-Peterson is slightly better than that of the Sips isotherm and followed by Langmuir, Temkin and Freundlich models. The Redlich-Peterson and Sips isotherm equations are extensions of the Langmuir model indicating that the adsorption sites are homogenous with monolayer coverage.

However, the best fit is the Redlich-Peterson and the Sips isotherm rather than the Langmuir isotherm indicating the adsorption was not achieved by a single identi-

Table 3. The calculated isotherm parameters and SSE for CBM adsorption

Model	Parameters and SSE	
Langmuir	q_m (mmol/g)	0.91
	k_L	0.39
	SSE	251
Freundlich	α_F (mmol/g) (L/mmol)	0.44
	$1/n_F$	0.18
	SSE	1100
Sips (Langmuir-Freundlich)	q_m (mmol/g)	0.88
	K_{LF} (L/g)	0.35
	n_{LF}	1.14
	SSE	232
Redlich-Peterson	q_m (mmol/g)	1.14
	K_R (L/g)	0.25
	β	1.06
	SSE	206
Temkin	RT/b_T	21.2
	A_T (L/ mmol)	1.25
	SSE	414

cal reaction, thus the adsorption of CBM may involve chemisorption on the surface of the adsorbent. Furthermore, since the point of zero charge (pH_{pzc}) of the adsorbent (activated at 900°C for 1.5 hours) was 11.5 and the pK_a of the CBM was 13.9, therefore, the CBM was in its neutral form and chemisorption may not be ascribed to ion exchange. The maximum adsorption capacity calculated from the Redlich-Peterson equation was 1.14 mmol/g which was considered very high in comparison with other adsorbents such as granular carbon nanotubes/alumina (157.4 $\mu\text{mol/g}$)^[26] and powdered activated carbon (0.179 $\mu\text{mol/g}$)^[27].

4 Conclusion

In this study, charred biomass, palm kernel shell (CPKS), was successfully modified by a physical method to produce an activated carbon material. The highest surface area and total porosity of 711.5 m^2/g and 42% can be achieved by treating the powdered size precursor (particle size ≤ 0.15 mm) at 900°C for 1.5 hour. Kinetic adsorption studies of carbamazepine (CBM) by activated CPKS were found to be efficient, within the first hour and reached equilibrium at 240 min. The adsorption process followed the Ritchie-second-order model indicating the chemisorption. The smallest SSE can be achieved by fitting the adsorption isotherm data with the Redlich-Peterson model followed by the Sips and Langmuir isotherms indicating the adsorbate and adsorbent interaction on the monolayer surface are not homogenous.

The high maximum adsorption capacity calculated from the Redlich-Peterson model equation was 1.14 mmol/g (268.7 mg/g), which is comparable with the commercial activated carbon.

Acknowledgement

The authors express their gratitude to Engineer Ronnie Ho, Peak Engineering Co., Limited, Hong Kong and Biomass Energy Co., Ltd. Jiangxi Peak, Pingxiang City, Jianxi Province, China., for providing the power station solid waste residue char samples from their Indonesian power generating facility for this research project.

References

- [1] Onundi YB, Mamun AA, Al Khatib MF, *et al.* Adsorption of copper, nickel and lead ions from synthetic semiconductor industrial wastewater by palm shell activated carbon. *International Journal of Environmental Science and Technology*, 2010, **7**(4): 751-758.
<https://doi.org/10.1007/BF03326184>
- [2] Hadi P, Barford J and McKay G. Toxic heavy metal capture using a novel electronic waste-based material-mechanism, modeling and comparison. *Environmental Science & Technology*, 2013, **47**: 8248-8255.
<https://doi.org/10.1021/es4001664>
- [3] Chen B, Hui CW and McKay G. Film-pore diffusion modeling and contact time optimization for the adsorption of dyestuffs on pith. *The Chemical Engineering Journal*, 2001, **84**(2): 77-94.
[https://doi.org/10.1016/S1385-8947\(01\)00193-0](https://doi.org/10.1016/S1385-8947(01)00193-0)
- [4] Jung C, Park J, Lim KH, *et al.* Adsorption of selected endocrine disrupting compounds and pharmaceuticals on activated biochars. *Journal of Hazardous Materials*, 2013, **263**(2): 702-710.
<https://doi.org/10.1016/j.jhazmat.2013.10.033>
- [5] Cheung C, Porter JF and McKay G. Sorption kinetic analysis for the removal of cadmium ions from effluents using bone char. *Water Research*, 2001, **35**(3): 605-612.
[https://doi.org/10.1016/S0043-1354\(00\)00306-7](https://doi.org/10.1016/S0043-1354(00)00306-7)
- [6] Ho YS, Porter JF and McKay G. Equilibrium isotherm studies for the sorption of divalent metal ions onto peat: copper, nickel and lead single component systems. *Water, air, and soil pollution*, **141**(1-4): 1-33.
<https://doi.org/10.1023/A:1021304828010>
- [7] Peng Y and Yang YR. Research progress and developing prospect of fly ash. *Resources Environment and Information Engineering*, 2019, **1**(1): 18-22.
<https://doi.org/10.2508/REIE.2019.01.002>
- [8] Olajire AA, Giwa AA and Bello IA. Competitive adsorption of dye species from aqueous solution onto melon husk in single and ternary dye systems. *International Journal of Environmental Science and Technology*, 2015, **12**(3): 939-950.
<https://doi.org/10.1007/s13762-013-0469-8>
- [9] Garcia-Nunez JA, Ramirez-Contreras NE, Rodriguez DT, *et al.* Evolution of palm oil mills into bio-refineries: Literature review on current and potential uses of residual biomass and effluents. *Resources, Conservation and Recycling*, 2016, **110**: 99-114.
<https://doi.org/10.1016/j.resconrec.2016.03.022>
- [10] Samarghandi M, Hadi M and McKay G. Breakthrough curve analysis for fixed bed adsorption of azo dyes using novel pine cone-derived active carbon. *Adsorption Science & Technology*, 2014, **32**(10): 791-806.
<https://doi.org/10.1260/0263-6174.32.10.791>
- [11] Valix M, Cheung WH and McKay G. Preparation of activated carbon using low temperature carbonisation and physical activation of high ash raw bagasse for acid dye adsorption. *Chemosphere*, 2004, **56**(5): 493-501.
<https://doi.org/10.1016/j.chemosphere.2004.04.004>
- [12] Choy KKH, Barford JP and McKay G. Production of activated carbon from bamboo scaffolding waste-process design, evaluation and sensitivity analysis. *Chemical Engineering Journal*, 2005, **109**(1-3): 147-165.
<https://doi.org/10.1016/j.cej.2005.02.030>
- [13] Mui ELK, Cheung WH, Valix M, *et al.* Dye adsorption onto char from bamboo. *Journal of Hazardous Materials*, 2010, **177**(1-3): 1001-1005.
<https://doi.org/10.1016/j.jhazmat.2010.01.018>
- [14] Lodeiro P, Kwan SM, Perez JT, *et al.* Novel Fe loaded activated carbons with tailored properties for As(V) removal: Adsorption study correlated with carbon surface chemistry. *Chemical Engineering Journal*, 2013, **215-216**: 105-112.
<https://doi.org/10.1016/j.cej.2012.11.052>
- [15] Gao X, Wu L, Li Z, *et al.* Preparation and characterization of high surface area activated carbon from pine wood sawdust by fast activation with H3PO4 in a spouted bed. *Journal of Material Cycles and Waste Management*, 2018, **20**(2): 925-936.
<https://doi.org/10.1007/s10163-017-0653-x>
- [16] Hadi P, Xu M, Lin CSK, *et al.* Waste printed circuit board recycling Techniques and product utilization. *Journal of Hazardous Materials*, 2015, **269**: 20-26.
<https://doi.org/10.1016/j.cej.2015.01.090>
- [17] Amouzgar P, Vakili M, Chan ES, *et al.* Effects of Beading Parameters for Development of Chitosan-Nano-Activated Carbon Biocomposite for Acetaminophen Elimination from Aqueous Sources. *Environmental Engineering Science*, 2017, **34**(11): 805-815.
<https://doi.org/10.1089/ees.2017.0031>
- [18] Bazargan A, Kostic M, Stamenkovic O, *et al.* A calcium oxide based catalyst derived from palm kernel gasification residues for biodiesel production. *Journal of Fuel*, 2015, **150**: 519-525.
<https://doi.org/10.1016/j.fuel.2015.02.046>
- [19] Lua AC and Guo J. Microporous Oil-Palm-Shell Activated Carbon Prepared by Physical Activation for Gas-Phase Adsorption. *Langmuir*, 2001, **17**(22): 7112-7117.
<https://doi.org/10.1021/la010290c>
- [20] Styszko K, Szczurowski J, Czuma N, *et al.* Adsorptive removal of pharmaceuticals and personal care products from aqueous solutions by chemically treated fly ash. *International Journal of Environmental Science & Technology*, 2018, **15**(3): 493-506.
<https://doi.org/10.1007%2F13762-017-1415-y>

- [21] Kara S, Aydiner C, Demirbas E, *et al.* Modeling the effects of adsorbent dose and particle size on the adsorption of reactive textile dyes by fly ash. *Desalination*, 2007, **212**(1-3): 282-293.
<https://doi.org/10.1016/j.desal.2006.09.022>
- [22] Lagergren SK. About the theory of so-called adsorption of soluble substances. *Sven. Vetenskapsakad. Handlingar*, 1898, **24**: 1-39.
- [23] Ho YS and McKay G. The kinetics of sorption of divalent metal ions onto sphagnum moss peat. *Water Research*, 2000, **34**(3): 735-742.
[https://doi.org/10.1016/S0043-1354\(99\)00232-8](https://doi.org/10.1016/S0043-1354(99)00232-8)
- [24] Ritchie AG. Alternative to the Elovic Equation for the Kinetics of Adsorption of Gases on Solids. *Journal of the Chemical Society Faraday Transactions 1*, 1977, **73**: 1650-1653.
<https://doi.org/10.1039/f19777301650>
- [25] Low MJD. Kinetics of Chemisorption of Gases on Solids. *Chemical Reviews*, 1960, **60**(3): 267-312.
<https://doi.org/10.1021/cr60205a003>
- [26] Suriyanon N, Punyapalaku P and Ngamcharussrivichai C. Mechanistic study of diclofenac and carbamazepine adsorption on functionalized silica-based porous materials. *The Chemical Engineering Journal*, 2013, **214**(1): 208-218.
<https://doi.org/10.1016/j.cej.2012.10.052>
- [27] Wei H, Deng S, Huang Q, *et al.* Regenerable granular carbon nanotubes/alumina hybrid adsorbents for diclofenac sodium and carbamazepine removal from aqueous solution. *Water Research*, 2013, **47**(12): 4139-4147.
<https://doi.org/10.1016/j.watres.2012.11.062>